Faraday Discussions

Cite this: *Faraday Discuss.*, 2017, **196**, 335

PAPER

AIE fluorophore with enhanced cellular uptake for tracking esterase-activated release of taurine and ROS scavenging†

Jun Wang,‡ Yinglong Wu,‡ Fang Zeng,* Shuailing Huang and Shuizhu Wu*

Received 6th May 2016, Accepted 14th June 2016
DOI: 10.1039/c6fd00118a

Fluorophores with aggregation-induced emission (AIE) characteristics are attractive and versatile tools for both chemical sensing and biological imaging. Herein, we designed and synthesized a fluorescent light-up system CTPE-Tau with enhanced cellular uptake ability. The system possesses several advantages, such as a large Stokes shift, low cytotoxicity, and good photostability. Also, it has been successfully utilized to track esterase-activated release of taurine and to scavenge intracellular ROS, and shows great potential for trackable visualized therapy.

Introduction

Fluorescence techniques have the characteristics of real-time response, high sensitivity and technical simplicity.[1–9] They have been successfully used in the fields of molecular recognition and biological imaging because of their flexible and diverse mechanisms.[10–21] Aggregation-induced emission (AIE), as an attractive luminescence mechanism, successfully solved the aggregation-caused quenching (ACQ)[22,23] problems of some organic dyes. These AIE fluorogens[24–26] are highly emissive in the aggregated state but non-emissive in dilute solutions,[27,28] which results from mechanisms involving restriction of intramolecular rotation (RIR) in the aggregation state and rapid intramolecular motion in solution. In addition, AIE fluorophores also exhibit high photostability and a large Stokes shift, which are beneficial for applications over a longer period and can avoid interference of background fluorescence in cell imaging. Recently, a class of organic luminogens with an extraordinary AIE feature[29,30] has opened new ways to

College of Materials Science and Engineering, State Key Laboratory of Luminescent Materials and Devices, South China University of Technology, Guangzhou 510640, P. R. China. E-mail: mcfzeng@scut.edu.cn; shzhwu@scut.edu.cn; Fax: +86 20 22236363; Tel: +86 20 22236262

† Electronic supplementary information (ESI) available: Stability experiments, ^{1}H NMR spectra, mass spectra, absorption emission spectra and cell imaging. See DOI: 10.1039/c6fd00118a

‡ These authors contributed equally to this work.

develop probes which are specifically responsive to biomolecules. Nevertheless, it is particularly important to develop new AIE fluorogens for visualized therapy.

Inflammation is a physiological response of tissues to harmful stimuli such as damaged cells, pathogens and irritants.[31] Inflammatory cells express excess hydrolytic enzymes[32] (esterase, protease and phosphatase) and are usually exposed to elevated levels of reactive oxygen species (ROS).[33] Overproduction of some ROS and insufficient neutralization by antioxidants may lead to the development of oxidative stress and chronic inflammation. As HClO/ClO^- (one of the most potent ROS) is highly reactive and diffusible,[34] its uncontrolled production within inflammatory cells is involved in a variety of human diseases,[35–39] such as inflammatory diseases and cardiovascular diseases.

Taurine (2-aminoethanesulfonic acid), which has been reported as an effective antioxidant, can protect tissues from oxidative stress associated with various inflammatory diseases. The best established antioxidant action of taurine is the elimination of hypohalous acids (HOCl, HOBr), the extremely toxic oxidants generated by the myeloperoxidase (MPO)–halide system.[40] Taurine reacts with HOCl/HOBr to produce taurine haloamines (TauCl/TauBr), which are less toxic milder oxidants but retain antimicrobial and anti-inflammatory properties. Although taurine is incapable of directly scavenging other classical ROS, it has been suggested that it is an effective inhibitor of ROS generation through enhancing expression and activities of antioxidant enzymes, such as superoxide dismutase, catalase and glutathione peroxidase.[41] Moreover, it has been recently reported that incorporating taurine can drastically boost cellular uptake for intracellular accumulation.[42]

In view of the above issues, we envision that combining hydrophilic taurine and an AIE fluorophore *via* an ester bond could turn out to be an elegant approach to extend the applications of AIE-active fluorophores, *e.g.* as a trackable visualized therapeutic system featuring both imaging esterase-activated taurine release and ROS scavenging. Herein we designed and synthesized a taurine-containing AIE fluorophore with a long Stokes shift (258 nm). This AIE fluorophore was coupled with a taurine moiety through a carbamate bond, and the hydrophilic taurine moiety enhanced its water solubility and cellular uptake ability. The ester bond can be hydrolysed by the overexpressed esterase in inflammatory cells, thereby releasing a taurine moiety for ROS scavenging and in the meantime an AIE fluorophore moiety as a reporter for tracking esterase-activated drug release, as shown in Scheme 1.

Experimental

Reagents and materials

Zinc powder, 4-hydroxybenzophenone, titanium tetrachloride (GR), tetrahydrofuran (THF for HPLC), 2-bromoethanol, caesium carbonate, *N*,*N*-dimethylformamide (DMF for HPLC), pyridine (for HPLC), acetate, malononitrile, tetrakis(triphenylphosphine)palladium(0), tetrabutylammonium bromide (TBAB for AR), and dimethylsulfoxide (DMSO for HPLC) were purchased from Aladdin and used as received. 4-Bromobenzophenone, 4-formylphenylboronic acid and 4-nitrophenyl chloroformate were purchased from TCI. 4-Dimethylaminopyridine (DMAP) was purchased from Alfa Aesar. Dichloromethane, hexane, methanol and other solvents were analytically pure reagents. Murine macrophage cells

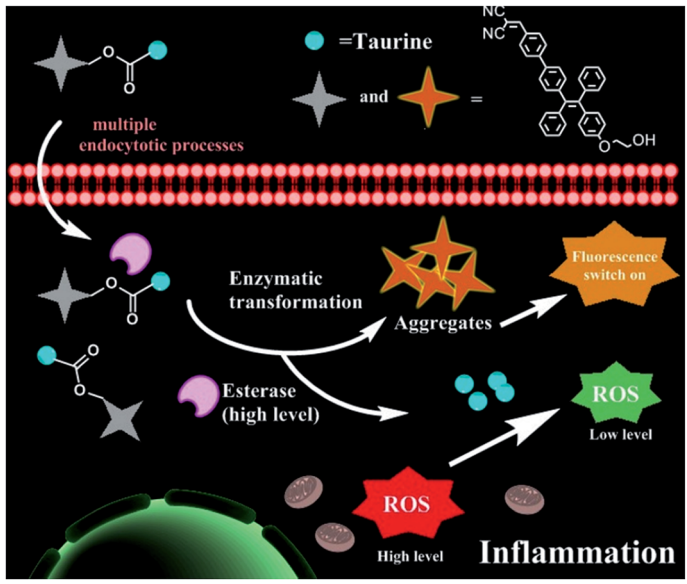

Scheme 1 Schematic illustration of cellular uptake for the system and the subsequent esterase-activated fluorescence switching on and ROS scavenging.

(RAW264.7) were purchased from KeyGen Biology Co. Ltd (Nanjing, China). Phorbol myristate acetate (PMA) was purchased from Abcam. DCFH-DA were purchased from Sigma-Aldrich. The water used herein was triply distilled water. RPMI1640 and antibiotics (penicillin and chloramphenicol) were purchased from Gibco. Fetal bovine serum (FBS) was obtained from Life Technologies.

Characterization

^{1}H NMR spectra were measured with a Bruker Avance 600 MHz NMR Spectrometer. Mass spectra were obtained using a Bruker Esquire HCT Plus mass spectrometer. UV-vis spectra were measured on a Hitachi U-3010 UV-vis spectrophotometer. Fluorescence spectra were measured using a Hitachi F-4600 fluorescence spectrophotometer. The particle size and distribution were determined through dynamic light scattering (DLS) using a Malvern Nano-ZS90 particle size analyzer at a fixed angle of 90° at 25 °C. Transmission electronic microscopy (TEM) experiments were performed by dropping a drop of the solution onto ultra-thin carbon film and observation was carried out with a JEM-2100F transmission electron microscope. Fluorescence images were obtained using an Olympus IX 71 with a DP72 color CCD.

Spectral analysis

Fluorescence spectra were recorded with an excitation of 369 nm. The stock solution was prepared by dissolving CTPE-Tau in DMSO and diluting with PBS buffer (10 mM, pH = 7.4) for absorbance or fluorescence spectra measurements.

For measurements of esterase-activated taurine release in buffer solutions, corresponding doses of esterase were added to CTPE-Tau in pH 7.4 PBS

containing 0.5% DMSO and maintained at 37 °C with a water bath. The fluorescence spectra were periodically recorded during incubation.

Synthesis

Synthesis of 4-(2-(4-bromophenyl)-1,2-diphenylvinyl)phenol (compound 3). Compound **3** was synthesized as reported in the literature[43] with a slight modification. In a nitrogen atmosphere, 4-hydroxybenzophenone (1.98 g, 10 mmol) and 4-bromobenzophenone (2.61 g, 10 mmol) were dissolved in 120 mL of THF in a 250 mL two-necked round-bottom flask. Zinc dust (3.8 g, 60 mmol) was subsequently added to the flask, followed by cooling with an ice bath. $TiCl_4$ (6.74 mL, 67.5 mmol) was added into the mixture dropwise with an injector. The reaction was then refluxed overnight under nitrogen. After the solution was cooled to room temperature, the THF was evaporated under reduced pressure. Saturated sodium bicarbonate solution was added to the mixture until no bubbles came out. The mixture was then extracted with dichloromethane and dried with anhydrous sodium sulfate. The crude product was purified using silica column chromatography, using hexane and dichloromethane (1 : 3 v/v), giving compound **3** as a white powder (1.8 g, 42%).

^{1}H NMR (600 MHz, DMSO), δ (ppm): 9.42–9.38 (d, 1H), 7.32–7.29 (d, 2H), 7.17–7.15 (d, 2H), 7.13–7.08 (m, 4H), 6.99–6.94 (m, 4H), 6.90–6.85 (m, 2H), 6.76–6.72 (m, 2H), 6.55–6.49 (q, 2H). MS (ESI): m/z 426.5 $[M]^-$.

Synthesis of 2-(4-(2-(4-bromophenyl)-1,2-diphenylvinyl)phenoxy)ethan-1-ol (compound 5). Into a 100 mL two-necked round-bottom flask was added compound **3** (1.3 g, 3 mmol) and caesium carbonate (1.76 g, 5.4 mmol). After 2-bromoethanol (0.42 mL, 6 mmol) and DMF (20 mL) were added, the flask was vacuumed and purged with nitrogen five times. The reaction was stirred overnight under nitrogen at 110 °C. After the mixture cooled to room temperature, it was extracted with dichloromethane, washed with distilled water several times and dried with anhydrous sodium sulfate. The crude product was purified using silica column chromatography with hexane and dichloromethane (1 : 3 v/v) to give compound **5** as a white solid (1.3 g, 92% yield). ^{1}H NMR (600 MHz, DMSO), δ (ppm): 7.36–7.30 (q, 2H), 7.21–7.08 (m, 7H), 6.99–6.92 (m, 4H), 6.90–6.84 (m, 3H), 6.74–6.68 (q, 2H), 4.83–4.80 (q, 1H), 3.92–3.88 (m, 2H), 3.69–3.64 (m, 2H).

Synthesis of 4′-(2-(4-(2-hydroxyethoxy)phenyl)-1,2-diphenylvinyl)-[1,1′-biphenyl]-4-carbaldehyde (compound 7). Compound **5** (0.94 g, 2 mmol) was dissolved in toluene (30 mL) in a 100 mL two-necked round-bottom flask followed by addition of 2 M potassium carbonate aqueous solution (8 mL). Tetrabutylammonium bromide (TBAB, 0.1 g, 0.3 mmol) and 4-formylphenylboronic acid (0.36 g, 2.4 mmol) were dissolved in the mixture. After the mixture was stirred at room temperature for 0.5 h, tetrakis(triphenylphosphine)palladium(0) ($Pd(Pph_3)_4$, 0.010 g, 8.7 nmol) was added. The flask was vacuumed and purged with nitrogen five times immediately and then heated to 90 °C for 24 h. After that the mixture was poured into ethyl acetate and washed three times with brine. The organic layer was dried over anhydrous sodium sulfate. After removing the solvent under reduced pressure, the residue was chromatographed on a silica gel column with dichloromethane and acetone (100 : 1 v/v) as eluent to give compound **7** (0.61 g, 62% yield). ^{1}H NMR (600 MHz, DMSO), δ (ppm): 10.02 (s, 1H), 7.95–7.94 (d, 2H), 7.86–7.85 (d, 2H), 7.58–7.56 (d, 2H), 7.19–7.17 (m, 3H), 7.15–7.12 (m, 3H),

7.08–7.06 (d, 2H), 7.04–7.02 (m, 4H), 6.87–6.86 (d, 2H), 6.71–6.69 (d, 2H), 4.83–4.81 (t, 1H), 3.90–3.89 (t, 2H), 3.68–3.65 (q, 2H). MS (ESI): m/z 518.9 $[M]^+$.

Synthesis of 2-((4′-(2-(4-(2-hydroxyethoxy)phenyl)-1,2-diphenylvinyl)-[1,1′-biphenyl]-4-yl)methylene)malononitrile (compound 9, CTPE). Compound 7 (0.3 g, 0.6 mmol), malononitrile (0.037 mL, 0.6 mmol), and pyridine (4 mL) were added to a 25 mL round-bottom flask with a stirrer bar. After acetic acid (0.16 mL) was added to the mixture, the mixture was warmed to 40 °C and maintained at this temperature overnight and the reaction was monitored several times using TLC, which showed that one orange product was formed as the only product. After that, the reaction product was dissolved with ethyl acetate, washed with 0.1 M hydrochloric acid solution 3 times and brine 1 time, dried over anhydrous sodium sulfate, and concentrated in a vacuum. The crude product was purified using silica column chromatography with dichloromethane and methanol (100 : 1 v/v) to give compound **9** as an orange solid (0.28 g, 86% yield). ^{1}H NMR (600 MHz, DMSO), δ (ppm): 8.56–8.54 (d, 1H), 8.05–8.01 (m, 2H), 7.93–7.90 (m, 2H), 7.76–7.61 (m, 2H), 7.32–7.28 (m, 2H), 7.19–7.06 (m, 8H), 6.99–6.97 (m, 2H), 6.93–6.86 (m, 2H), 6.74–6.69 (m, 2H), 4.80–4.61 (m, 1H), 3.95–3.89 (m, 2H) 3.69–3.66 (m, 2H). MS (ESI): m/z 566.9 $[M]^+$.

Synthesis of 2-(4-(2-(4′-(2,2-dicyanovinyl)-[1,1′-biphenyl]-4-yl)-1,2-diphenylvinyl)-phenoxy)ethyl(4-nitrophenyl) carbonate (compound 11). To a suspension of 4-nitrophenylchloroformate (0.1 g, 0.5 mmol) and DMAP (0.06 g, 0.5 mmol) in dichloromethane (10 mL) was added compound **9** (0.22 g, 0.4 mmol) dissolved in CH_2Cl_2 (15 mL) dropwise. Then the reaction was stirred for 3 h at room temperature. After completion, silica column chromatography using dichloromethane and methanol (100 : 1 v/v) was carried out to remove the excess raw material. The crude product was concentrated in a vacuum and used for the next step without further purification.

Synthesis of 2-(((2-(4-(2-(4′-(2,2-dicyanovinyl)-[1,1′-biphenyl]-4-yl)-1,2-diphenylvinyl)phenoxy)ethoxy)carbonyl)amino)ethane-1-sulfonic acid (compound 13, CTPE-Tau). The crude ester intermediate compound **11** was immediately reacted with taurine (0.1 g, 0.8 mmol) in dry CH_2Cl_2 (30 mL) containing 0.3 mL dry Et_3N. After 1 day of reaction, the mixture was washed with brine and dried with anhydrous sodium sulfate. The solvent was removed under reduced pressure. The crude product was purified using silica column chromatography with dichloromethane and methanol (10 : 1 v/v) to give compound **13** as an orange solid (0.12 g, 40% yield). ^{1}H NMR (600 MHz, DMSO), δ (ppm): 8.02–7.85 (m, 4H), 7.62–7.57 (m, 2H), 7.20–7.12 (m, 8H), 7.08–7.07 (d, 2H), 7.04–7.02 (t, 5H), 6.87–6.86 (m, 2H), 6.73–6.71 (d, 2H), 4.21–4.14 (m, 2H), 4.05–4.00 (m, 2H), 3.27–3.24 (m, 2H), 2.58–2.55 (t, 2H). MS (ESI): m/z 694.3 $[M]^-$.

Cell viability evaluated with MTT assay

To examine the cytotoxicity of CTPE-Tau, RAW264.7 cells (murine macrophage cells) were seeded in 96-well plates at a density of 1×10^5 cells per mL in complete medium, which was composed of 89% RPMI1640 medium with 10% fetal bovine serum (FBS) and 1% antibiotics (penicillin and chloramphenicol) added. The cells were incubated at 37 °C with 5% CO_2 for 24 h. After removal of the medium and washing with PBS buffer, the cells were treated with a series of concentrations of CTPE-Tau and incubated for an additional 24 h. Then the freshly prepared MTT

solution was added to each sample well after being washed with PBS. After 3 h incubation in the incubator, the MTT medium solution was carefully removed. DMSO (100 μL) was then added into each well and the plate was gently shaken for 10 min at room temperature to dissolve all the precipitates formed. The evaluation of cytotoxicity for CTPE-Tau against the cells was obtained with MTT assay according to ISO 10993-5. The absorbance of MTT of every individual well at 570 nm was monitored and the cell viability was calculated using the ratio of the absorbance in the sample well to that of the incubated cells with culture medium only. In these experiments for each concentration the assays were performed in eight replicates. The evaluation of cell viability was expressed using the statistical mean and standard deviation.

Cell incubation and imaging

For cellular uptake imaging, Raw 264.7 cells were seeded in polylysine-coated cell culture glass slides inside 30 mm glass culture dishes in complete medium. After being grown for 24 h for adherence at 37 °C in a humidified 5% CO_2 incubator, the cells were washed with PBS and incubated with 50 μM of corresponding CTPE or CTPE-Tau in complete medium at 37 °C under 5% CO_2 for 4 h. Then the cells were washed with PBS buffer three times and the glass slides were taken out to image using an Olympus IX71 inverted fluorescence microscope equipped with a DP72 color CCD.

For cellular ROS scavenging imaging, Raw 264.7 cell lines were seeded in polylysine-coated cell culture glass slides inside 30 mm glass culture dishes in complete medium. After being grown for 24 h for adherence at 37 °C in a humidified 5% CO_2 incubator, the cells were washed with PBS.

For comparison, experiments concerning four groups of cells were conducted: for the first group (DCFH-DA only), cells were incubated in complete medium at 37 °C in a humidified 5% CO_2 incubator; after that, the cells were incubated with DCFH-DA at a final concentration of 10 μM for 30 min. For the second group (PMA/DCFH-DA), cells were stimulated with 6 mg mL^{-1} PMA dissolved in complete medium for 30 min in an incubator; afterwards, the cells were washed with PBS and incubated for 4 h in complete medium only; then the cells were incubated with DCFH-DA at a final concentration of 10 μM for 30 min. For the third group (PMA/CTPE-Tau/DCFH-DA), cells were stimulated with 6 mg mL^{-1} PMA dissolved in complete medium for 30 min in an incubator; afterwards, the cells were washed with PBS 3 times and incubated with CTPE-Tau in complete medium at a final concentration of 50 μM for 4 h at 37 °C in a humidified 5% CO_2 incubator; then the cells were incubated with DCFH-DA at a final concentration of 10 μM for 30 min. For the fourth group (PMA/taurine/DCFH-DA), cells were stimulated with 6 mg mL^{-1} PMA dissolved in complete medium for 30 min in an incubator; after that, the cells were washed with PBS 3 times and incubated with taurine in complete medium at a final concentration of 50 μM for 4 h at 37 °C in a humidified 5% CO_2 incubator; then the cells were incubated with DCFH-DA at a final concentration of 10 μM for 30 min.

After all these incubations, the cells were washed with PBS buffer three times and the glass slides were taken out to image using an Olympus IX71 inverted fluorescence microscope equipped with a DP72 color CCD.

Results and discussion

Synthesis

CTPE-Tau was prepared following the synthetic route shown in Scheme 2: first, compound **3** was prepared by the cross McMurry coupling reaction of 4-hydroxybenzophenone and 4-bromobenzophenone. Second, the Williamson ether synthesis reaction between compound **3** and 2-bromoethanol in the presence of caesium carbonate catalyst led to the product compound **5** with >90% yields. This reaction was employed because it may decrease the steric hindrance as a substrate of esterase. Third, compound **5** was transformed to compound **7** using a Suzuki coupling reaction with 4-formylphenylboronic acid. Fourth, the subsequent condensation between compound **7** and malononitrile gave compound **9** (CTPE). Fifth, the nucleophilic substitution reaction between compound **9** and 4-nitrophenylchloroformate gave compound **11**. Sixth, the nucleophilic substitution reaction between intermediate **11** and taurine give the final product compound **13** (CTPE-Tau).

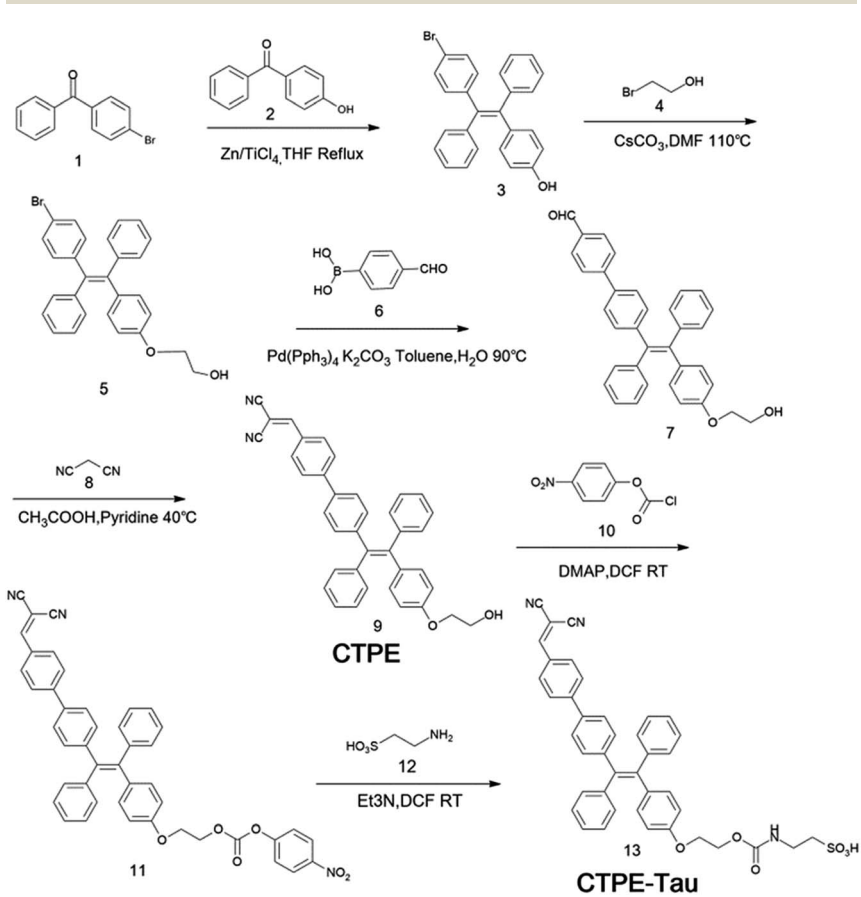

Scheme 2 Synthetic route for CTPE-Tau.

^{1}H NMR and mass spectrometry (MS) were utilized to characterize the intermediates and CTPE-Tau and satisfactory results corresponding to their structures were obtained (Fig. S1–S9†). Furthermore, a high resolution mass spectrum (HRMS) was obtained for CTPE-Tau (Fig. S10†).

Optical properties

The fluorophore was designed under the rationale of incorporating a donor–π–acceptor structure as well as extending the conjugation length. The bathochromic shift compared with the TPE in emission (around 470 nm) results from the strong donor–acceptor interaction across the TPE core, which facilitates the intramolecular charge transfer (ICT) and lowers the energy gap. The AIE properties of CTPE and CTPE-Tau were studied by monitoring their fluorescence emission spectra in water and DMSO mixtures with different water fractions (f_w). For both samples, we observed a broad emission band centered around 609 nm. As shown in Fig. 1A and B, CTPE is almost non-emissive in DMSO solution ($f_w = 0$), which accounts for the free rotation of the TPE phenyl rings in the molecularly dissolved state. However, the fluorescence intensity increases with the increase in f_w within

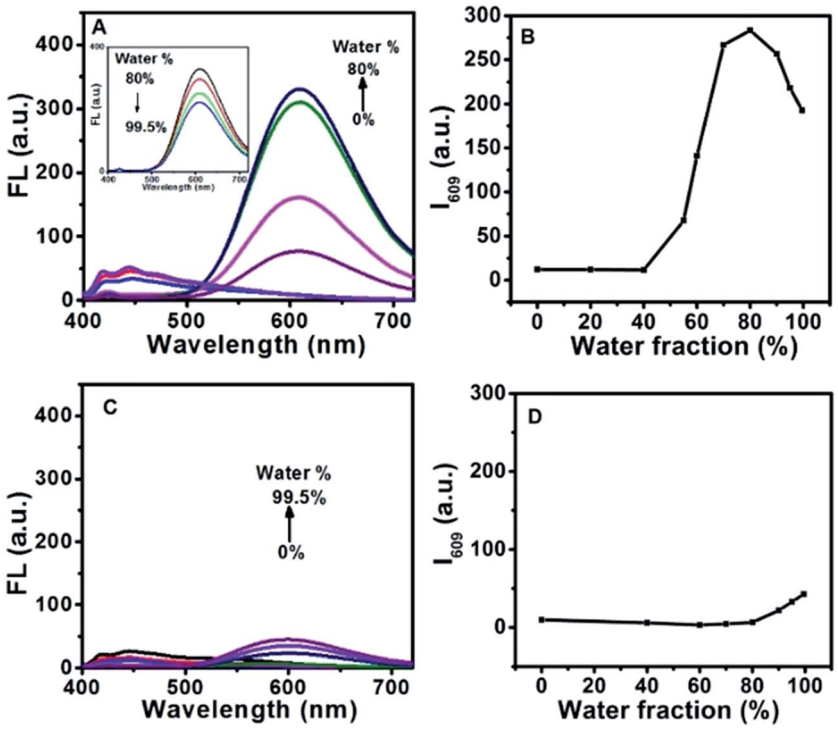

Fig. 1 (A) FL spectra of CTPE in H_2O/DMSO mixtures with different H_2O fractions. Concentration: 10 μM; excitation wavelength: 369 nm. (B) Plot of FL intensity (I609) *versus* composition of the H_2O/DMSO mixture of CTPE. (C) FL spectra of CTPE-Tau in H_2O/DMSO mixtures with different H_2O fractions. Concentration: 10 μM; excitation wavelength, 369 nm. (D) Plot of FL intensity (I609) *versus* composition of the H_2O/DMSO mixture of CTPE-Tau.

the range from 0% to 80%. At $f_w = 80\%$, the fluorescence intensity of CTPE is 24-fold higher than that in DMSO. This should be explained by the fact that hydrophobic CTPE tends to aggregate at a higher water fraction, which leads to restriction of the intramolecular motion to activate the AIE process. However the FL intensity shows a decreasing trend when f_w ranges from 80% to 99.5%. This results from the ratio changes of the amorphous and crystalline phases of the compounds.[44]

Additionally, fluorophores with small Stokes shifts may suffer from self-quenching and larger measurement error due to overlap between the excitation and emission bands, whereas those with larger Stokes shift could help to reduce the excitation interference and increase the contrast between the target fluorescence signal and other background fluorescence.

Compared with other reported fluorescent probes (see ESI Table S1†), the system herein can respond to esterase with subsequent drug release (taurine) and have a large Stokes shift. As a result, this large Stokes shift (258 nm) of the fluorophore is highly desirable for cell imaging applications (Fig. S11†).

CTPE-Tau was obtained by coupling CTPE with a taurine moiety through a carbamate bond. The taurine moiety greatly improves the water solubility of the AIE fluorophore. Therefore, as shown in Fig. 1C and D, CTPE-Tau exhibits weak fluorescence emission even when f_w reaches up to 99.5%. This phenomenon can be attributed to CTPE-Tau's relatively good water solubility where the intramolecular rotation of the compound serves as a relaxation channel for the excited state.

The photostability of a fluorophore is one of the key parameters for applications. The fluorescence intensity of the fluorophore CTPE is relatively stable in PBS from pH = 5.0 to pH = 8.0 and remains almost unchanged even after 4 hours heating at 37 °C with a water bath (Fig. S12A†), which means that the optical properties of CTPE will not be affected by the pH of the environment. In addition, we measured the change in fluorescence intensity of CTPE with different irradiation times. It can be seen in Fig. S12B† that there is only slight photobleaching upon exposure to 365 nm UV for at least 60 minutes, which suggests that the fluorophore has relatively good photostability, which is beneficial for fluorescence imaging. These characteristics lay a solid foundation for the fluorophore's application in biological systems.

Esterase-activated release of taurine

To investigate the esterase-activated taurine release, we measured the fluorescence spectra of CTPE-Tau towards esterase *in vitro*. Firstly, we investigated whether acidic pH affects the hydrolysis of carbamate. CTPE-Tau (10 μM) was incubated in pH = 5.0 (the pH in cell lysosome) PBS containing 0.5% DMSO for different time periods. The fluorescence intensity shows no enhancement under such acidic conditions (Fig. S13†), which indicates that CTPE-Tau will not hydrolyse under the acidic environment in the cell lysosome. Then we tested response of CTPE-Tau towards esterase at different concentrations at 37 °C, and the fluorescence spectra were periodically recorded during incubation (CTPE-Tau 10 μM in PBS containing 0.5% DMSO). For esterase at 0.05 mg mL^{-1},[45] which was reported previously to control prodrug release in live cells, the fluorescence intensity reaches a plateau in 10 min (Fig. 2B). As shown in Fig. 2A, in the absence

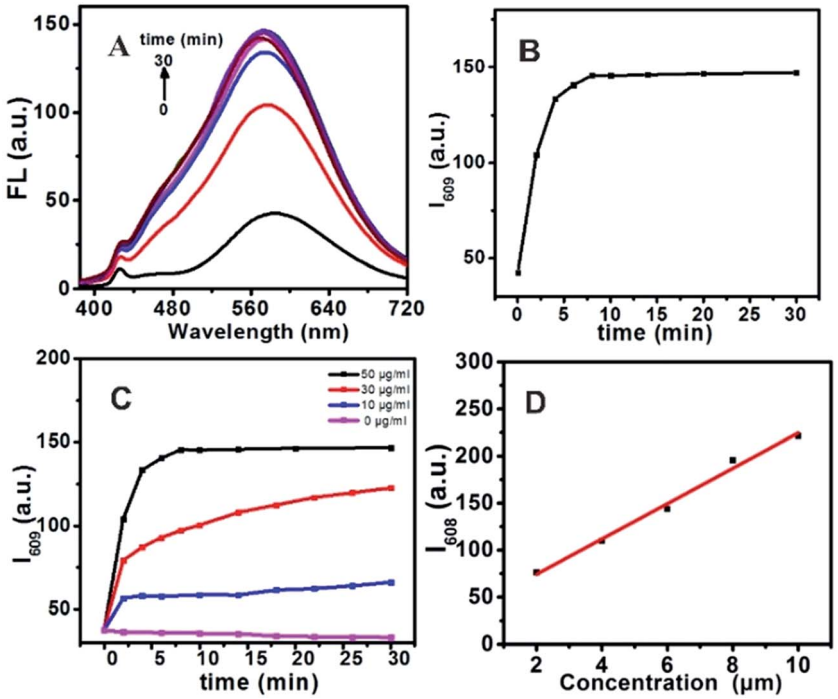

Fig. 2 (A) FL spectra of CTPE-Tau for esterase response *versus* time. (B) Fluorescence intensity of CTPE-Tau in the presence of esterase 0.05 mg mL^{-1} as a function of time, and (C) upon incubation with esterase at different concentrations (CTPE-Tau 10 μM in PBS containing 0.5% DMSO). (D) The working curve of the fluorescence intensity against CTPE concentration in the range of 2–10 μM. These measurements were performed in PBS (pH 7.4) at 37 °C with $\lambda_{ex/em}$ = 369/609 nm.

of esterase, CTPE-Tau shows weak emission at 609 nm for its non-aggregated state. On adding esterase and increasing the esterase incubation time, the fluorescence intensity of the assay system at 609 nm increases as water-soluble CTPE-Tau is gradually hydrolysed into hydrophobic CTPE. The resulting hydrophobic CTPE molecules in the test solution readily aggregate. The restriction of intramolecular rotation (RIR) holds back the non-radiative way and opens up a radiative channel.[21] As a result, the system becomes emissive. Higher concentrations of esterase lead to a faster hydrolysis rate and a higher hydrolysis degree, as shown in Fig. 2C. The mass spectrum (Fig. S14†) indicated that free taurine was generated by CTPE-Tau after incubation with esterase (MS (ESI): m/z 124.9 $[M]^+$).

Next, to investigate the release efficiency of taurine activated by esterase, we tested the relationship between CTPE concentration and its fluorescence intensity and obtained the working curve. It can be seen in Fig. 2D that the enhancement of emission could serve as a useful reporter for drug release with a linear equation of $F = 18.8C$ (μM) + 36.6 ($R = 0.995$). The release rate is determined to be 60% for esterase at 0.05 mg mL^{-1}, calculated based on the working curve in Fig. 2D.

In addition, we studied the size change of the system before and after esterase incubation using DLS and TEM at the same time. The system has an average diameter of about 1 nm before adding esterase. After the addition and incubation

of esterase for 30 min, the size of the system grows to about 105 nm as shown in Fig. 3C and D. TEM images show that there are no obvious aggregates before the addition of esterase (Fig. 3A), whereas the size of the system grows to about 83 nm (Fig. 3B) after the incubation of esterase for 30 min, which corresponds to the DLS results. These results illustrate that after being hydrolyzed to CTPE, the system indeed aggregates.

Fluorescence cell imaging

In order to examine the enhanced cellular uptake capability as well as the ability to track the release of taurine and scavenging ROS, we selected RAW264.7 cells, one of the inflammatory cell lines, for an *in vitro* assay. Cytotoxicity assays were firstly performed on a RAW 264.7 cell line with MTT assay in compliance with ISO 10993-5 with CTPE-Tau at concentrations in the range of 0 and 50 μM for 24 h. As shown in Fig. 4, CTPE-Tau has little cytotoxicity. Notably, even at higher concentrations reaching up to 50 μM, the viability of the cell line is still about 90%. These results demonstrate that CTPE-Tau possesses good biocompatibility and is appropriate for applications in live cells.

To prove that coupling with the taurine moiety can enhance cellular uptake, we compared the cellular uptake ability of CTPE-Tau with CTPE. RAW 264.7 cells

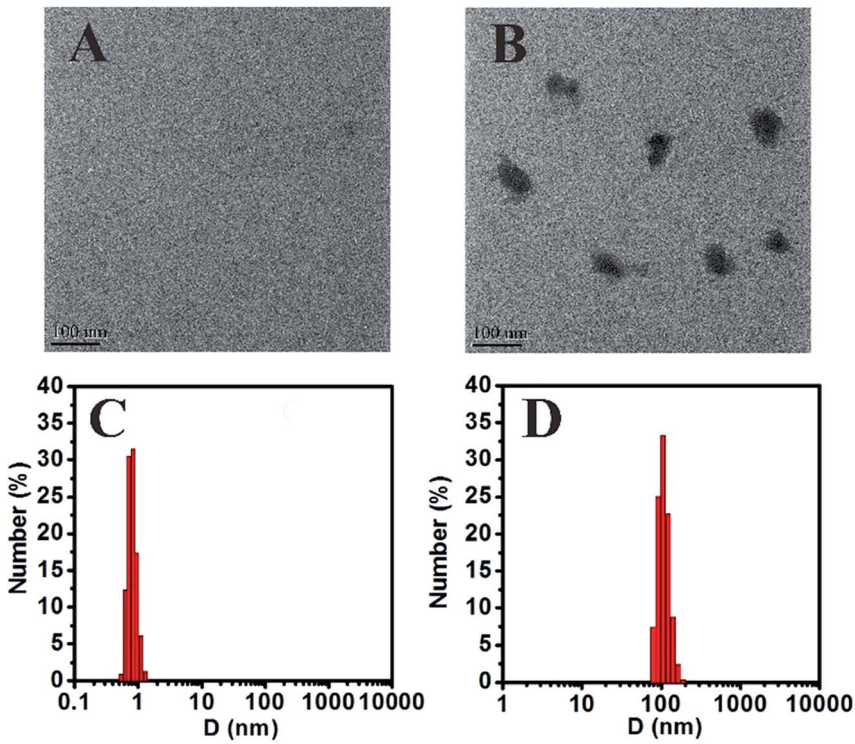

Fig. 3 TEM images of the assay systems before (A) and after (B) the addition of esterase. Scale bar: 100 nm. Size distribution of CTPE-Tau determined using dynamic light scattering (DLS) before (C) and after (D) treatment with esterase (10 μM in PBS containing 0.5% DMSO).

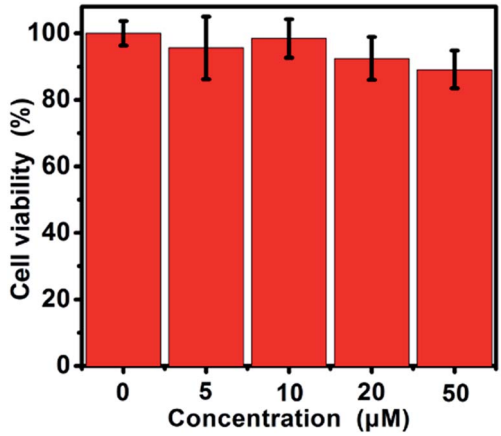

Fig. 4 Cytotoxic assays against RAW264.7 cells upon 24 hours of incubation with different CTPE-Tau concentrations (0, 5, 10, 20, 50 μM).

were incubated with CTPE-Tau and CTPE at the same concentration (50 μM) for 4 h. Theoretically speaking, the fluorescence intensity of CTPE-Tau should be weaker than CTPE if the cells take in the same amount of the two substances, CTPE and CTPE-Tau. That is because CTPE-Tau has almost no fluorescence emission properties as previously described and may not be completely hydrolyzed into bright CTPE by the esterase inside the cells. But surprisingly, the fluorescence imaging experiments show a clear fluorescence enhancement for

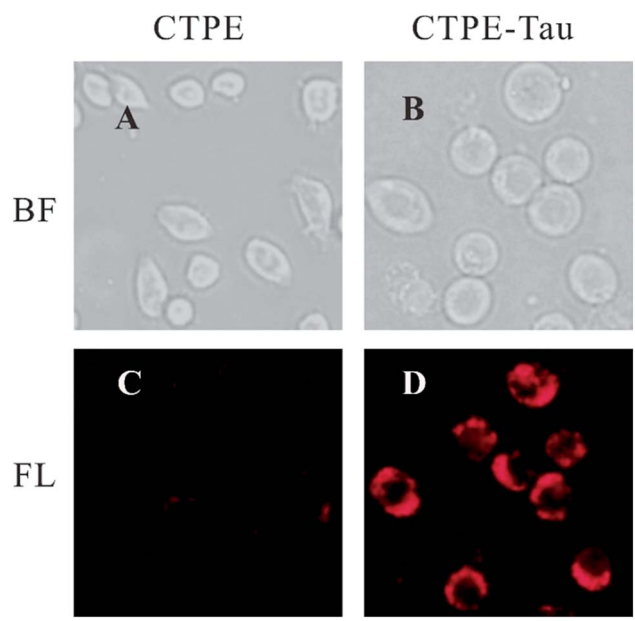

Fig. 5 Fluorescence images of RAW 264.7 cells incubated with (A, C) CTPE and (B, D) CTPE-Tau, both at 50 μM for 4 h in the same conditions.

CTPE-Tau compared to CTPE with an accumulation in the cytoplasm (Fig. 5). This result indicates that coupling with the taurine moiety indeed boost cellular uptake.

Next we investigated the ROS-scavenging ability of CTPE-Tau. It has been reported that murine macrophage cells RAW264.7 secrete myeloperoxidase (MPO) and that exposure of macrophages to stimuli such as phorbol myristate acetate (PMA) can generate ROS[46,47] by activating NADPH oxidase to produce O^{2-} which is then converted to H_2O_2 and subsequently into HClO by MPO. In this experiment, we used PMA-stimulated RAW 264.7 cells[48] as a model to test the ROS-scavenging ability of CTPE-Tau. The level of cellular ROS is characterized by DCFH-DA, a commonly used cell membrane-permeable fluorescent indicator for ROS.[49] DCFH-DA is weakly fluorescent but could react with ROS to yield the strong green, fluorescent dichlorofluorescein (DCF).[50]

We can see from the results in Fig. S15† that the DCFH-DA only group (Fig. S15A and C†) shows no fluorescence while the PMA/DCFH-DA group (Fig. S15B and D,† Fig. 6C and I) shows strong DCF green fluorescence, which indicates that the level of cellular ROS in RAW264.7 cells increases tremendously upon stimulation by PMA. After treating the high ROS level cells with CTPE-Tau or taurine, the strong DCF fluorescence decreases dramatically (PMA/CTPE-Tau/DCFH-DA group, Fig. 6A and G and PMA/taurine/DCFH-DA group, Fig. 6B and H) because the ROS is scavenged by taurine. In addition, we can monitor the esterase-activated taurine release *via* the fluorescence of the resulting CTPE. These results indicate that CTPE-Tau is capable of scavenging intracellular ROS due to the taurine it releases upon esterase activation. Meanwhile, the bright red

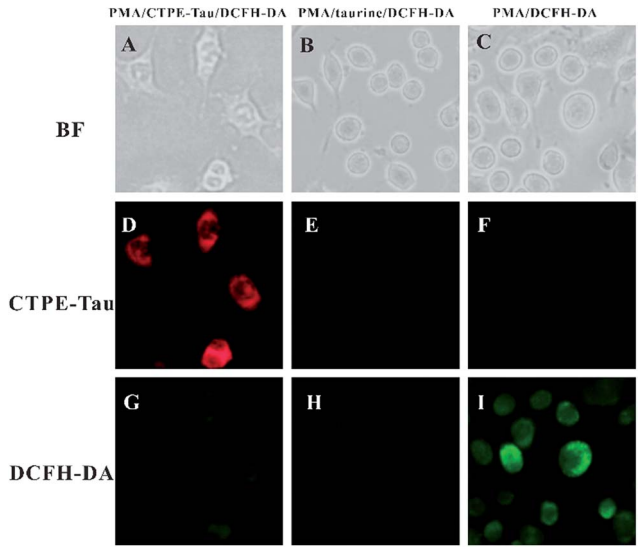

Fig. 6 Fluorescence images of RAW 264.7 cells: (A, D, G) stimulated with 6 mg mL^{-1} PMA for 30 min, washed with PBS 3 times and incubated with 50 μM CTPE-Tau for 4 h followed by DCFH-DA 10 μM for 30 min; (B, E, H) stimulated with 6 mg mL^{-1} PMA for 30 min, washed with PBS 3 times and incubated with 50 μM taurine for 4 h followed by DCFH-DA 10 μM for 30 min; (C, F, I) stimulated with 6 mg mL^{-1} PMA for 30 min, washed with PBS 3 times and incubated in culture medium for 4 h followed by DCFH-DA 10 μM for 30 min.

fluorescence of the hydrolyzed CTPE-Tau, namely the CTPE aggregates (Fig. 6D), is able to serve as an indicator for tracking taurine release.

Conclusions

In summary, we have successfully designed an AIE fluorophore with a large Stokes shift (258 nm), and this fluorophore CTPE-Tau was obtained by coupling the taurine moiety through an ester bond to the AIE fluorophore which enhanced its water solubility and cellular uptake capability. Furthermore, the antioxidant taurine can be released upon activation by esterase which is overexpressed in inflammatory cells. In addition, the released hydrophobic CTPE can act as a fluorescent reporter to track taurine release *via* aggregation-induced emission. Moreover, CTPE-Tau has been successfully used to scavenge intracellular ROS and for imaging in live cells. Our approach herein may offer helpful insights for designing other trackable therapeutic systems.

Acknowledgements

We gratefully acknowledge the financial support from the National Key Basic Research Program of China (Project no. 2013CB834702), NSFC (21574044, 21474031 and 21174040), the Science and Technology Planning Project of Guangdong Province (Project No. 2014A010105009) and the Fundamental Research Funds for the Central Universities (2015ZY013).

Notes and references

1 J. Chan, S. C. Dodani and C. J. Chang, *Nat. Chem.*, 2012, **4**, 973–984.
2 L. A. Juarez, A. M. Costero, M. Parra, S. Gil, F. Sancenon and R. Martinez-Manez, *Chem. Commun.*, 2015, **51**, 1725–1727.
3 X. Kuang, Y. Ma, C. Zhang, H. Su, J. Zhang and B. Tang, *Chem. Commun.*, 2015, **51**, 5955–5958.
4 J. H. Lee, J. H. Jang, N. Velusamy, H. S. Jung, S. Bhuniya and J. S. Kim, *Chem. Commun.*, 2015, **51**, 7709–7712.
5 S. Guo, F. Zheng, F. Zeng and S. Z. Wu, *Chin. J. Polym. Sci.*, 2016, **34**, 830–837.
6 C. Yu, X. Li, F. Zeng, F. Zheng and S. Z. Wu, *Chem. Commun.*, 2013, **49**, 403–405.
7 C. Yu, Y. Wu, F. Zeng, X. Li, J. Shi and S. Z. Wu, *Biomacromolecules*, 2013, **14**, 4507–4514.
8 K. Adamson, E. Spain, U. Prendergast, R. J. Forster, N. Moran and T. E. Keyes, *Biomater. Sci.*, 2014, **2**, 1509.
9 J. Ling, G. Naren, J. Kelly, A. Qureshi and A. P. de Silva, *Faraday Discuss.*, 2015, **185**, 337–346.
10 A. Akdeniz, L. Mosca, T. Minami and P. Anzenbacher Jr, *Chem. Commun.*, 2015, **51**, 5770–5773.
11 Y. Ding, Y. Tang, W. Zhu and Y. Xie, *Chem. Soc. Rev.*, 2015, **44**, 1101–1112.
12 D. Lee, G. Kim, J. Yin and J. Yoon, *Chem. Commun.*, 2015, **51**, 6518–6520.
13 D. T. Shi, D. Zhou, Y. Zang, J. Li, G. R. Chen, T. D. James, X. P. He and H. Tian, *Chem. Commun.*, 2015, **51**, 3653–3655.
14 B. Y. Wu and X. P. Yan, *Chem. Commun.*, 2015, **51**, 3903–3906.

15 Z. Zhang, J. Huang, B. Dong, Q. Yuan, Y. He and O. S. Wolfbeis, *Nanoscale*, 2015, **7**, 4149–4155.
16 X. Hou, Q. Yu, F. Zeng, J. Ye and S. Wu, *J. Mater. Chem. B*, 2015, **3**, 1042–1048.
17 J. Ding, H. Li, C. Wang, J. Yang, Y. Xie, Q. Peng, Q. Li and Z. Li, *ACS Appl. Mater. Interfaces*, 2015, **7**, 11369–11376.
18 S. Y. Xu, X. Sun, H. Ge, R. L. Arrowsmith, J. S. Fossey, S. I. Pascu, Y. B. Jiang and T. D. James, *Org. Biomol. Chem.*, 2015, **13**, 4143–4148.
19 H. Y. Au-Yeung, J. Chan, T. Chantarojsiri and C. J. Chang, *J. Am. Chem. Soc.*, 2013, **135**, 15165–15173.
20 X. P. He and H. Tian, *Small*, 2016, **12**, 144–160.
21 S. U. Hettiarachchi, B. Prasai and R. L. McCarley, *J. Am. Chem.Soc.*, 2014, **136**, 7575–7578.
22 J. Mei, N. L. Leung, R. T. Kwok, J. W. Lam and B. Z. Tang, *Chem. Rev.*, 2015, **115**, 11718–11940.
23 M. Gao, Q. Hu, G. Feng, B. Z. Tang and B. Liu, *J. Mater. Chem. B*, 2014, **2**, 3438.
24 X. Tang, Q. Bai, Q. Peng, Y. Gao, J. Li, Y. Liu, L. Yao, P. Lu, B. Yang and Y. Ma, *Chem. Mater.*, 2015, **27**, 7050–7057.
25 Z. Liu, W. Xue, Z. Cai, G. Zhang and D. Zhang, *J. Mater. Chem.*, 2011, **21**, 14487.
26 G. Liu, D. Chen, L. Kong, J. Shi, B. Tong, J. Zhi, X. Feng and Y. Dong, *Chem. Commun.*, 2015, **51**, 8555–8558.
27 F. Hu, G. Zhang, C. Zhan, W. Zhang, Y. Yan, Y. Zhao, H. Fu and D. Zhang, *Small*, 2015, **11**, 1335–1344.
28 J. Yang, J. Huang, N. Sun, Q. Peng, Q. Li, D. Ma and Z. Li, *Chemistry*, 2015, **21**, 6862–6868.
29 Y. Gao, Y. Qu, T. Jiang, H. Zhang, N. He, B. Li, J. Wu and J. Hua, *J. Mater. Chem. C*, 2014, **2**, 6353.
30 Z. Wang, L. Yan, L. Zhang, Y. Chen, H. Li, J. Zhang, Y. Zhang, X. Li, B. Xu, X. Fu, Z. Sun and W. Tian, *Polym. Chem.*, 2014, **5**, 7013–7020.
31 K. Ewa, P. Magdalena, L. Barbara, O. Malgorzata, M. Pawel and M. Wlodzimierz, *Ann. Rheum. Dis.*, 2012, **71**, 262–267.
32 Y. Wu, S. Huang, F. Zeng, J. Wang, C. Yu, J. Huang, H. Xie and S. Wu, *Chem. Commun.*, 2015, **51**, 12791–12794.
33 J. Marcinkiewicz and E. Kontny, *Amino Acids*, 2014, **46**, 7–20.
34 J. Fan, H. Mu, H. Zhu, J. Du, N. Jiang, J. Wang and X. Peng, *Ind. Eng. Chem. Res.*, 2015, **54**, 8842–8846.
35 J. T. Hou, K. Li, J. Yang, K. K. Yu, Y. X. Liao, Y. Z. Ran, Y. H. Liu, X. D. Zhou and X. Q. Yu, *Chem. Commun.*, 2015, **51**, 6781–6784.
36 L. Long, Y. Wu, L. Wang, A. Gong, F. Hu and C. Zhang, *Chem. Commun.*, 2015, **51**, 10435–10438.
37 S. I. Reja, V. Bhalla, A. Sharma, G. Kaur and M. Kumar, *Chem. Commun.*, 2014, **50**, 11911–11914.
38 Y. Wu, J. Wang, F. Zeng, S. Huang, J. Huang, H. Xie, C. Yu and S. Z. Wu, *ACS Appl. Mater. Interfaces*, 2016, **8**, 1511–1519.
39 H. Xiao, K. Xin, H. Dou, G. Yin, Y. Quan and R. Wang, *Chem. Commun.*, 2015, **51**, 1442–1445.
40 H. Zhu, J. Fan, J. Wang, H. Mu and X. Peng, *J. Am. Chem. Soc.*, 2014, **136**, 12820–12823.
41 S. J. Jin, P. Shuyu, C. Young-Nam and K. Chaekyun, *J. Clin. Biochem. Nutr.*, 2009, **45**, 37–43.

42 J. Zhou, X. Du, J. Li, N. Yamagata and B. Xu, *J. Am. Chem. Soc.*, 2015, **137**, 10040–10043.
43 E. Zhao, Y. Chen, H. Wang, S. Chen, J. W. Lam, C. W. Leung, Y. Hong and B. Z. Tang, *ACS Appl. Mater. Interfaces*, 2015, **7**, 7180–7188.
44 Q. Lu, X. Li, J. Li, Z. Yang, B. Xu, Z. Chi, J. Xu and Y. Zhang, *J. Mater. Chem. C*, 2015, **3**, 1225–1234.
45 G. Pan, S. Liu, X. Zhao, J. Zhao, C. Fan and W. Cui, *Biomaterials*, 2015, **53**, 202–210.
46 Y. Yi-Cyun, L. Hsueh-Han, W. Wei-Ti and L. Ian, *Anal. Chem.*, 2011, **83**, 8267–8272.
47 T. Salonen, O. U. Sareila, H. Kankaanranta, R. Tuominen and E. Moilanen, *Br. J. Pharmacol.*, 2006, **147**, 790–799.
48 B. Wang, P. Li, F. Yu, P. Song, X. Sun, S. Yang, Z. Lou and K. Han, *Chem. Commun.*, 2013, **49**, 1014–1016.
49 M. Karlsson, T. Kurz, U. T. Brunk, S. E. Nilsson and C. I. Frennesson, *Biochem. J.*, 2010, **428**, 183–190.
50 Y. Yuan, S. Xu, C.-J. Zhang, R. Zhang and B. Liu, *J. Mater. Chem. B*, 2016, **4**, 169–176.